Copy
RM L53I29

NACA RM L53I29

7483

NACA

RESEARCH MEMORANDUM

RESULTS OF A ROCKET-MODEL INVESTIGATION OF CONTROL-SURFACE

BUZZ AND FLUTTER ON A 4-PERCENT-THICK UNSWEPT WING

AND ON 6-, 9-, AND 12-PERCENT-THICK SWEPT

WINGS AT TRANSONIC SPEEDS

By Allen B. Henning

Langley Aeronautical Laboratory
Langley Field, Va.

CLASSIFIED DOCUMENT

NATIONAL ADVISORY COMMITTEE
FOR AERONAUTICS
WASHINGTON
November 20, 1953

NACA RM L53I29

NATIONAL ADVISORY COMMITTEE FOR AERONAUTICS

RESEARCH MEMORANDUM

RESULTS OF A ROCKET-MODEL INVESTIGATION OF CONTROL-SURFACE

BUZZ AND FLUTTER ON A 4-PERCENT-THICK UNSWEPT WING

AND ON 6-, 9-, AND 12-PERCENT-THICK SWEPT

WINGS AT TRANSONIC SPEEDS

By Allen B. Henning

SUMMARY

The results of an investigation of control-surface buzz and flutter on four rocket-powered models having a 4-percent-thick unswept wing and 6-, 9-, and 12-percent-thick 35° swept wings with free-floating and statically mass-balanced control surfaces are herein presented. These results show that all the control surfaces buzzed. The control-surface buzz is related to the presence of a shock wave near the control surface for subsonic speeds. Coupling of the control-surface buzz with wing motion occurred near the wing first-bending frequency on the swept wings, whereas on the unswept wing it occurred at an intermediate frequency between bending and torsion. Wing thickness is an important factor in that an increase in thickness increased the amplitude of the buzz. The amplitude of the control-surface buzz tended to decrease with an increase in Mach number at supersonic speeds. The frequency of the control-surface vibration decreased with a decrease in air density.

INTRODUCTION

Since the advent of high-speed aircraft much interest has been shown concerning control-surface buzz which is a type of one-degree-of-freedom flutter with the control surface oscillating about the hinge line. Several studies have been made of this phenomenon. A test on a wing of a fighter plane was made in the Ames 16-foot high-speed wind tunnel under a constant-density condition. This test showed that there was a distinct relationship between the control-surface movement and the motion of the shock wave on the wing (ref. 1). Other tests were made in the Langley $4\frac{1}{2}$-foot flutter research tunnel on a different type of wing and control surface (ref. 2). The difference in density was found to have little

effect on the amplitude and on the Mach number associated with the control-surface oscillation; however, it was found that the frequency of the oscillation decreased with a decrease in density. In reference 3, it was stated that the presence of a shock wave can lead to a control-surface buzz which can occur without any motion of the wing.

This paper presents the data from four rocket-powered, free-flight, control-surface buzz models each having a wing of different thickness. Each model had a control surface in one of its three wings that was statically mass-balanced and completely unrestrained so that it was free floating.

The models were test flown at the Langley Pilotless Aircraft Research Station at Wallops Island, Va.

SYMBOLS

A	aspect ratio, $\dfrac{b^2}{S}$
b	twice the semispan of the wing, ft
c	wing chord, ft
c_a	control-surface chord, ft
C_D	drag coefficient based on total exposed wing area, $\dfrac{\text{Drag}}{qS'}$
C_p	pressure coefficient, $\dfrac{p - p_0}{q}$
f	flutter frequency, cps
I_β	moment of inertia of control surface about hinge line, slug-ft^2
$1/k$	reduced velocity parameter, $\dfrac{2V}{c_a \omega}$
M	free-stream Mach number
p_0	free-stream static pressure, lb/sq ft
p	static pressure on airfoil, lb/sq ft

q   dynamic pressure, lb/sq ft

R   Reynolds number

S   total area of two wing panels to the center line, sq ft

S'   total exposed area of three wing panels, sq ft

t   time, sec

t/c   thickness of airfoil in percent of chord

V   free-stream velocity, ft/sec

δ control-surface deflection, deg

$\Delta\delta$ total amplitude, deg

θ/m wing stiffness parameter, wing torsion displacement made by
            a moment applied at tip of wing, radians/ft-lb

λ taper ratio, the wing-tip chord divided by the wing-root chord

Λ angle of sweep at 0.25 chord, deg

ρ density of air, slugs/cu ft

ω flutter circular frequency, $2\pi f$, radian/sec

MODELS AND TESTS

Models

     In the tests performed four models were used. Three of these models
had wings with 35° sweep and one model had an unswept wing. Figures 1
and 2 show drawings of a typical swept-wing model and the unswept-wing
model as well as detail drawings of the wing and control surface for each
of the two types of models. Photographs of the models are shown as
figures 3 and 4.

The airfoil used on all models was the NACA 65A-series parallel to the free stream. Each model had an airfoil of different thickness as follows:

Model	Airfoil	Λ
1	NACA 65A004	0°
2	NACA 65A006	35°
3	NACA 65A009	35°
4	NACA 65A012	35°

The basic construction for the bodies of each of these models was similar. They had a parabolic nose made of clear plastic with a cylindrical duralumin afterbody. Three wings were built into this body and one of these wings included a test control surface. The wings of model 1 were constructed of 24ST aluminum alloy and those of models 2, 3, and 4 were constructed of aircraft spruce with 24ST aluminum-alloy inlays. In figure 5 the wing stiffness parameter θ/m is plotted against the wing span for each model. In the swept-wing models the thicker the airfoil, the stiffer the wing. Because the wing of model 1 was so thin, solid aluminum construction was used; therefore, the wing of model 1 was stiffer than model 2. The wing vibration characteristics, which were measured in the laboratory, are shown in table I for each model. Wing A refers to the semispan wing that has the control surface and wing B and C refers to the other semispan wings that do not have the control surface. The natural frequency of the semispan wings and the nodal lines for these frequencies are given in table I.

The control surfaces were statically balanced about their hinge line and free to rotate between stops in an arc of ±15°. The control surface of the unswept-wing model had counter weights for mass-balancing that extended approximately 0.20 inches above the surface of the wing when fully deflected and was supported by three small journal-type bearings. The control surfaces of the swept models had a mass-balancing overhang of 21.5 percent of its chord and were supported by two small journal-type bearings. On each model the bearings were made as friction free as possible and the gaps between the wings and the control surfaces were approximately 0.03 inch. The complete control-surface data are given in table II.

Instrumentation

Each of the four models contained two instruments, a longitudinal accelerometer and a control-position indicator. The longitudinal accelerometer was located in the nose and used to measure the drag of the model, and a control-position indicator was used to indicate the position of the control surface at any time. In addition to these instruments, model 1 $\left(\Lambda = 0^\circ, \frac{t}{c} = 0.04\right)$ also contained two pressure cells that were located in the fuselage near the wing root and used to measure the static pressure at two points on the wing. These points were located on the same chord line at 27.7 percent of the exposed semispan. One point was located at 60 percent of the chord and the other point was located at 77.5 percent of the chord which was immediately in front of the control surface.

The velocity and position in space of the models were determined by means of CW Doppler radar and SCR 584 tracking radar, respectively. Spinsonde records were taken during the flights to determine the amount of roll on each model. Atmospheric conditions were determined from radiosonde observations made immediately after the model test flights.

Tests

Figure 6 shows a photograph of a typical booster-model combination mounted on a rail launcher. The models were boosted to supersonic speeds by 5-inch high-velocity aircraft rockets. After booster burnout, the booster separated from the model at which time the modified British cordite sustainer rocket motors fired accelerating the models to maximum speed. In each test the angle of attack was near zero. The rate of spin of all the models was low, the maximum helix angle was on the order of 0.005 radian.

Figure 7 shows a plot of the Reynolds number against Mach number. The Reynolds number for all the models falls within the envelope shown in this plot.

RESULTS AND DISCUSSION

This section, "Results and Discussion," is divided into three parts. These parts are buzz, which describes the action of the control surfaces and the wings; trim, which shows the angular position of the control surfaces; and the drag.

Buzz

Figure 8 gives a time-history account of the aileron behavior during the flights of each model. Mach number, total control-surface amplitude, and control-surface frequency are plotted against time. Table III summarizes the flutter frequencies and Mach number range of flutter. Buzz is considered to be the vibratory motion of the control surface without any motion of the wing. When the accelerometer shows any appreciable disturbance at the same instance and with the same vibration frequency of the control surface, an assumption is made that the control-surface buzz is coupled with a wing flutter mode.

Model 1 $\left(\Lambda = 0^\circ, \frac{t}{c} = 0.04\right)$ had one mode of vibration, and the frequency of that mode was on the order of 130 cycles per second. This vibration occurred during a short period of time and over a short Mach number range. The frequency of vibration does not correspond to either of the wing natural frequencies even though the accelerometer vibrated at the same frequency as the control surface.

Model 2 $\left(\Lambda = 35^\circ, \frac{t}{c} = 0.06\right)$ had three modes of vibration. The low frequency was between 52 and 59 cycles per second on the same order as the first bending mode for that wing. This vibration came during acceleration between Mach numbers of 0.784 and 0.915. The longitudinal accelerometer vibrated along with the control surface at the same frequency. The frequency of the next mode was between 116 and 123 cycles per second. This vibration was noted during acceleration between Mach numbers of 1.090 and 1.237. The accelerometer did not vibrate with the control surface. The amplitude of this vibration was low and on the order of 1.5°. The third mode of vibration for model 2 had a frequency between 206 and 290 cycles per second. This vibration was noted during deceleration between the Mach number of 1.129 and 0.700. The accelerometer did not vibrate with the control surface during this vibration mode either. The amplitude of this vibration was extremely small, being under 1°.

Model 3 $\left(\Lambda = 35^\circ, \frac{t}{c} = 0.09\right)$ had two modes of vibration. The low-frequency mode was between 69 and 72 cycles per second and occurred between Mach numbers of 0.540 and 0.644 during deceleration. This frequency was near the wing first-bending mode, and while the control surface was vibrating the accelerometer was also vibrating. The other mode of vibration was between 90 and 140 cycles per second during acceleration and deceleration through the transonic range without any longitudinal accelerometer disturbance.

Model 4 $\left(\Lambda = 35^\circ, \frac{t}{c} = 0.12\right)$ also had two modes of vibration. The low vibration was between 50 and 90 cycles per second during deceleration

and between the Mach numbers of 0.842 and 0.945. This low frequency was near the wing first-bending mode and the longitudinal accelerometer vibrated at the same frequency. The other mode of vibration for model 4 had a frequency from 105 to 140 cycles per second which occurred in the transonic speed range during acceleration and deceleration. There was no accelerometer disturbance during this vibration.

On swept wings each case of control-surface buzz coupled with a wing flutter mode occurred at the wing first-bending frequency, whereas for the unswept wing it occurred at an intermediate frequency between bending and torsion. These flutter modes appear to be excited by the control-surface oscillations.

Figures 9 to 11 are reproductions of sections of the actual telemeter records obtained from models 1, 3, and 4 and show clearly what happened when the control surface was oscillating. The buzz for model 1 $\left(\Lambda = 0^\circ,\right.$ $\left.\frac{t}{c} = 0.04\right)$ is shown in figure 9. The static-pressure measurements indicate the position of the shock wave relative to the motion of the control surface. As the shock wave passes over the wing it passes over pressure orifice 1 first and then over pressure orifice 2. (See figs. 3(b) and 1(b).) Orifice 2 is immediately in front of the control surface, and as the shock wave passes over this orifice and comes in contact with the control surface the control surface begins to buzz. Thus, the control-surface buzz is related to the presence of the shock wave over the surface. This result is in agreement with reference 1. The length of time of the buzz was 0.18 second; the amplitude, on the order of 8°; the Mach number, between 0.968 and 0.997; and the frequency, about 130 cycles per second. After the buzzing stopped, the control surface assumed a different angle of trim.

While the control surface was vibrating on the model, the longitudinal accelerometer showed some disturbance. The movement of the control surface could have excited the wing control-surface flutter mode which would cause the model to shake and disturb the accelerometer. This disturbance stopped when the buzz stopped. When the model passed through this same speed region during deceleration, no disturbance was noted on either the control surface or the accelerometer. The acceleration was 6.83 times that of gravity, and the deceleration was -2.61 times that of gravity, both measured at the same Mach number.

Sections from the telemeter record for model 3 $\left(\Lambda = 35^\circ, \frac{t}{c} = 0.09\right)$ are shown in figure 10. Figure 10(a) shows the start of control-surface buzz for this model at a Mach number of 0.883. It started abruptly and immediately jumped to a high total amplitude of 16° and a frequency of 140 cycles per second. After a sudden buildup the amplitude dropped down to around 9° while the frequency decreased. The model gained in

velocity until booster burnout where the Mach number was 1.137. There was no change in the nature of the buzz during the change from acceleration to deceleration. Figure 10(b) shows another section from the record of model 3 at the point where the sustainer fired. The Mach number at the time when the sustainer fired was 0.990. Again there was no change in the nature of the buzz due to a sudden change in the sense of the acceleration. The amplitude had increased slightly to 10.5° at the time the sustainer fired, and the frequency of the buzz continued to decrease slightly. Figure 10(c) shows the point at which the control-surface buzz stopped on model 3. The frequency had dropped to 103 cycles per second and the amplitude had decreased to 8.85°. The buzzing stopped at a Mach number of 0.934, and the abruptness at which the buzz stopped can be seen quite plainly. The control surface trimmed at a value of 0.3° after the surface had stopped vibrating. Throughout the flight of this model in the transonic-speed range there was no large amplitude oscillation of the longitudinal accelerometer; therefore, during this part of the flight there apparently was no occurrence of wing flutter.

A section from the telemeter record of model 4 $\left(\Lambda = 35^{\circ}, \frac{t}{c} = 0.12\right)$ is shown in figure 11. This section shows the longitudinal accelerometer vibrating along with the control surface. The control-surface frequency was steadily decreasing until it approached the natural frequency of the wing. At this point the vibration of the control surface excited the wing to vibrate at its natural frequency. The accelerometer and the control surface oscillated at 72 cycles per second which corresponds to the natural bending frequency of the wing. The oscillations stopped at a Mach number of 0.897 and started again at a Mach number of 0.866. When the accelerometer and control surface started to vibrate again the frequency was 63 cycles per second for both. The amplitude of these vibrations was on the order of 29° for the control surface. These excessive vibrations evidently caused the control surface to break away from the model; thus, more data could not be obtained.

The records obtained from model 2 $\left(\Lambda = 35^{\circ}, \frac{t}{c} = 0.06\right)$ were similar to those shown in figure 10 and are not reproduced here.

The various flutter regions mentioned in the foregoing paragraphs are shown graphically in figures 12 and 13 for models 2, 3, and 4 $(\Lambda = 35^{\circ})$. The reduced velocity parameter $1/k$ is plotted against density in figure 12. At various points on these plots the Mach numbers are given for reference. For these three models the buzz frequency was such that the value of $1/k$ was generally around 16. For model 2 $\left(\frac{t}{c} = 0.06\right)$ this value was attained during acceleration, but during coasting the control surface vibrated at a higher frequency to give a $1/k$ value of about 6. Although this frequency was high, the amplitude was very low. By placing

a straight edge at the same Mach number points on the plots for models 3 and 4 $\left(\frac{t}{c} = 0.09 \text{ and } 0.12\right)$ it can be seen that at a constant Mach number the frequency of vibration decreased with a decrease in density. This result would substantiate the findings of reference 2. The plots for models 3 and 4 also show that near the end of the buzz pattern the frequency decreased sharply before the buzz stopped. This decrease in frequency was from the order of 105 cycles per second to around 90 cycles per second.

The amplitude of the control-surface buzz is plotted against Mach number in figure 13(a). The amplitude for model 4 was quite high and near the deflection limit of the control. This plot shows that at supersonic speeds an increase in speed generally resulted in a decrease in amplitude. Figure 13(b) shows the amplitude plotted against the reduced-velocity parameter. The reduced velocity increased with a decrease in amplitude due to the velocity effects even though the actual frequency of the control surface decreased. From figures 13(a) and 13(b) it can be seen that with an increase in thickness of the airfoil there is a decided increase in the amplitude of the buzz.

Trim

The trim angle of the control surfaces for each model is shown plotted against Mach number in figure 14. In each case the trim values were obtained by fairing a line through the oscillation; therefore, the absolute angles are only approximately defined but trends with Mach number are evident. The trim angle change of model 1 $\left(\Lambda = 0^{\circ}, \frac{t}{c} = 0.04\right)$ and model 3 $\left(\Lambda = 35^{\circ}, \frac{t}{c} = 0.09\right)$ from subsonic speeds to supersonic speed was small and without any large irregularities. Model 2 $\left(\Lambda = 35^{\circ}, \frac{t}{c} = 0.06\right)$ had abrupt and large changes both for acceleration and deceleration. Model 4 $\left(\Lambda = 35^{\circ}, \frac{t}{c} = 0.12\right)$ had the same angle of trim for both acceleration and deceleration in the supersonic speed range, but transonically the change was quite irregular. During the coasting period through the transonic region the erratic behavior of the control surface of model 4 can possibly be due to the high amplitude of vibration.

The pressure coefficients from the two points on the wing of model 1 $\left(\Lambda = 0^{\circ}, \frac{t}{c} = 0.04\right)$ are plotted against Mach number in figure 15.

Drag

The drag coefficient for all models, based on the total exposed wing area, is plotted against Mach number in figure 16. Models 2, 3, and 4 ($\Lambda = 35°$) have the same wing area. The increase in drag from one model to the next shows the influence of thickness on the drag. The drag of model 4 with a 12-percent-thick wing is twice as much as that for model 2 with a 6-percent-thick wing at supersonic speeds.

CONCLUSIONS

From the investigation of control-surface buzz and flutter on a 4-percent-thick unswept wing and 6-, 9-, and 12-percent-thick swept wings with free-floating and statically mass-balanced control surfaces, these conclusions can be made:

1. The 4-percent-thick unswept wing and the 6-, 9-, and 12-percent-thick swept wing all encountered control-surface buzz.

2. The unswept-wing pressure measurements showed that the control-surface buzz was related to the presence of the shock wave over the surface for subsonic speeds. This result is in agreement with results obtained in NACA RM A7F30 and Jour. Royal Aero. Soc, May 1952.

3. At subsonic speeds, longitudinal accelerometer vibrations accompanied the control-surface buzz near the wing first-bending frequency for the swept wings and at an intermediate frequency between first bending and torsion for the unswept wing. This result is interpreted to indicate an appreciable coupling of the wing motion with the control-surface buzz.

4. These tests are in agreement with those obtained in NACA RM L9B08 in that the frequency of the control-surface vibration decreased with a decrease in air density.

5. The amplitude of the control-surface buzz tended to decrease with an increase in Mach number at supersonic speeds.

6. The wing thickness is an important factor in that for an increase in thickness there is an increase in the amplitude of the buzz.

Langley Aeronautical Laboratory,
    National Advisory Committee for Aeronautics,
        Langley Field, Va., September 10, 1953.

REFERENCES

1. Erickson, Albert L., and Stephenson, Jack D.: A Suggested Method of Analyzing for Transonic Flutter of Control Surfaces Based on Available Experimental Evidence. NACA RM A7F30, 1947.

2. Clevenson, Sherman A.: Some Wind-Tunnel Experiments on Single Degree of Freedom Flutter of Ailerons in the High Subsonic Speed Range. NACA RM L9B08, 1949.

3. Broadbent, E. G. and Kirkby, W. T.: Control Surface Flutter. Jour. R.A.S., vol. LVI, May 1952, pp. 355-375. Discussion: pp. 375-381.

TABLE I.- WING CHARACTERISTICS

Model	t/c, percent chord	A	λ	Λ, deg	Weight, lb		Natural frequency, cps				Location of node lines, —— Wing A - - - Wing B and C
							Wing A		Wing B and C		
					Wing A	Wing B and C	Torsion	Bending	Torsion	Bending	
1	0.04	4	0.6	0	3.3	2.7	280	55	234	56	First bending / Torsion
2	0.06	3.43	0.75	35	2.1	1.7	173	43	243	56	First bending / Torsion
3	0.09	3.43	0.75	35	2.2	1.8	420	87	350	87	First bending / Torsion
4	0.12	3.43	0.75	35	3.0	2.4	238	72	422	95	First bending / Torsion
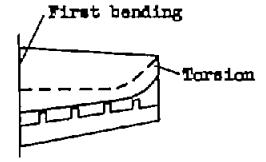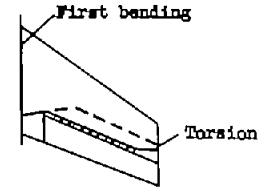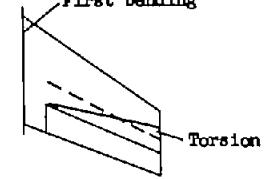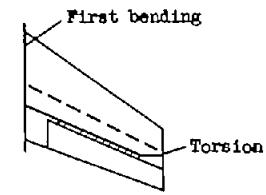
TABLE II.- CONTROL-SURFACE DATA

Model	Wing thickness	Type of control surface	Static balance, percent	Weight of control surface, lb	Moment of inertia of control surface, slug-ft^2	Gap, percent wing chord
1	0.04	Full span	100	0.25	1.736×10^{-5}	0.36
2	.06	0.82 span	100	.472	1.980×10^{-5}	.30
3	.09	.82 span	100	.607	2.285×10^{-5}	.30
4	.12	.82 span	100	.745	2.620×10^{-5}	.30

TABLE III.- SUMMARY OF FLUTTER FREQUENCIES AND MACH NUMBER RANGE

Model	Flutter frequency, cps	Mach number range of flutter
1	130	0.968 to 0.997
2	52 to 59	.784 to .915
	116 to 123	1.090 to 1.237
	206 to 290	.700 to 1.129
3	69 to 72	.540 to .644
	90 to 140	.903 to 1.20
4	50 to 90	.842 to .945
	105 to 140	.945 to 1.238

Top view

66.75

25-percent wing chord line

90°

Wing A

47.35

6.5 diam.

17.5 R

Wing B and C

Side view

End view
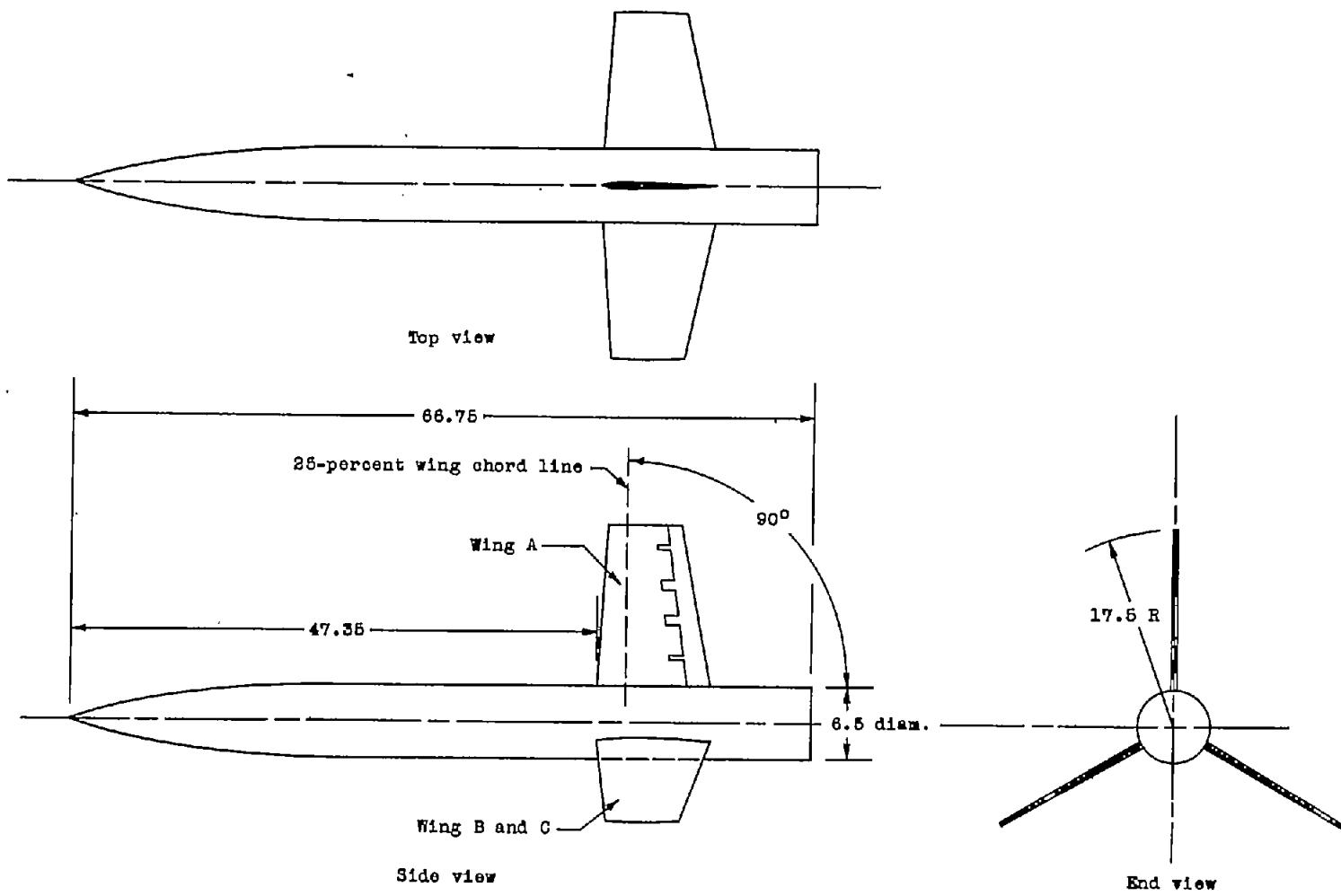
(a) Three-view drawing.

Figure 1.- Detail drawing of unswept-wing model. All dimensions are in inches. See figure 1(b) for detail drawing of wing.

CONFIDENTIAL
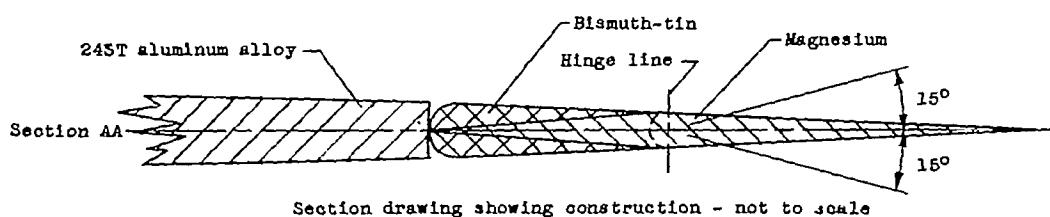
Section drawing showing construction - not to scale
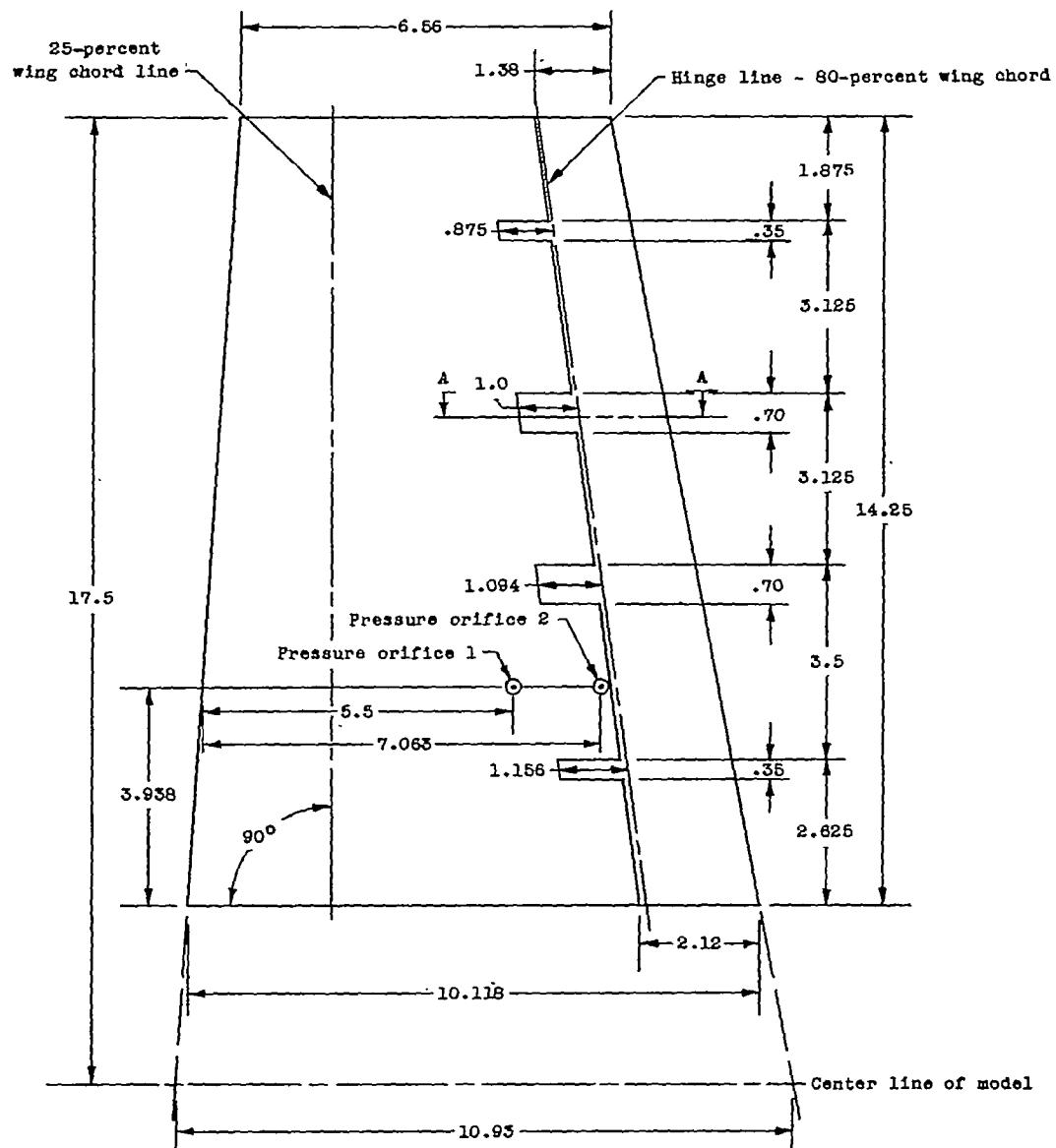
(b) Plan form of unswept wing with control surface.

Figure 1.- Concluded.

3U

Top view

66.75

35°

35-percent wing chord line

Wing A

17.5 R

47.375

6.5 diam.

Wing B and C

Side view

End view
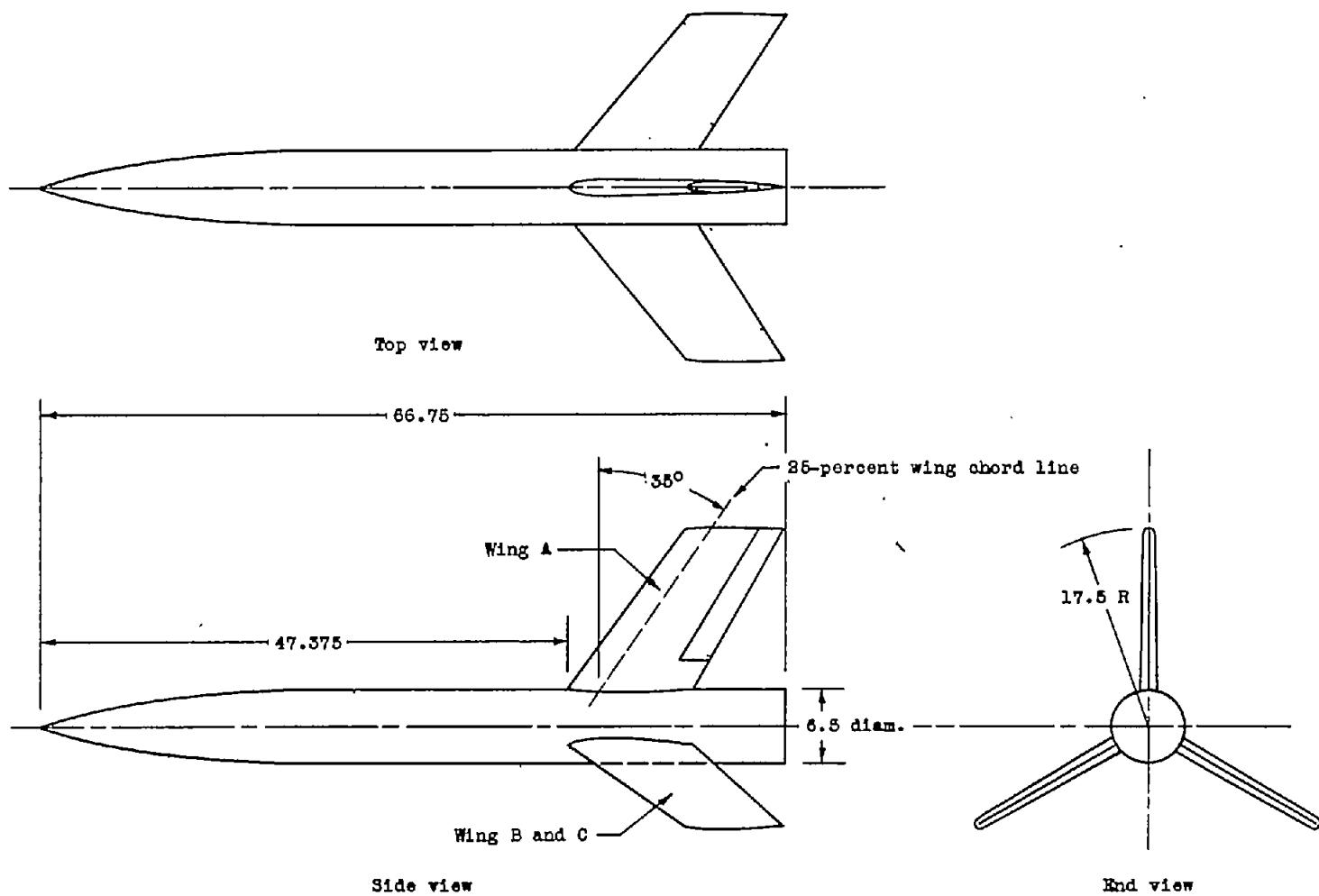
(a) Three-view drawing.

Figure 2.- Detail drawing of typical swept-wing model. All dimensions
are in inches. See figure 2(b) for detail drawing of wing.

0.016 - 24ST aluminum alloy

Hinge line

Bismuth-tin

0.004 brass sheet

15°

15°

Section AA

Spruce

Brass

Balsa

Brass tubing

Section drawing showing construction - not to scale

8.75

6.52

2.23

Hinge line - 80-percent wing chord

25-percent wing chord line

A

A

11.67

14.25

17.5

35°

2.72

11.135

Center line of model

11.67
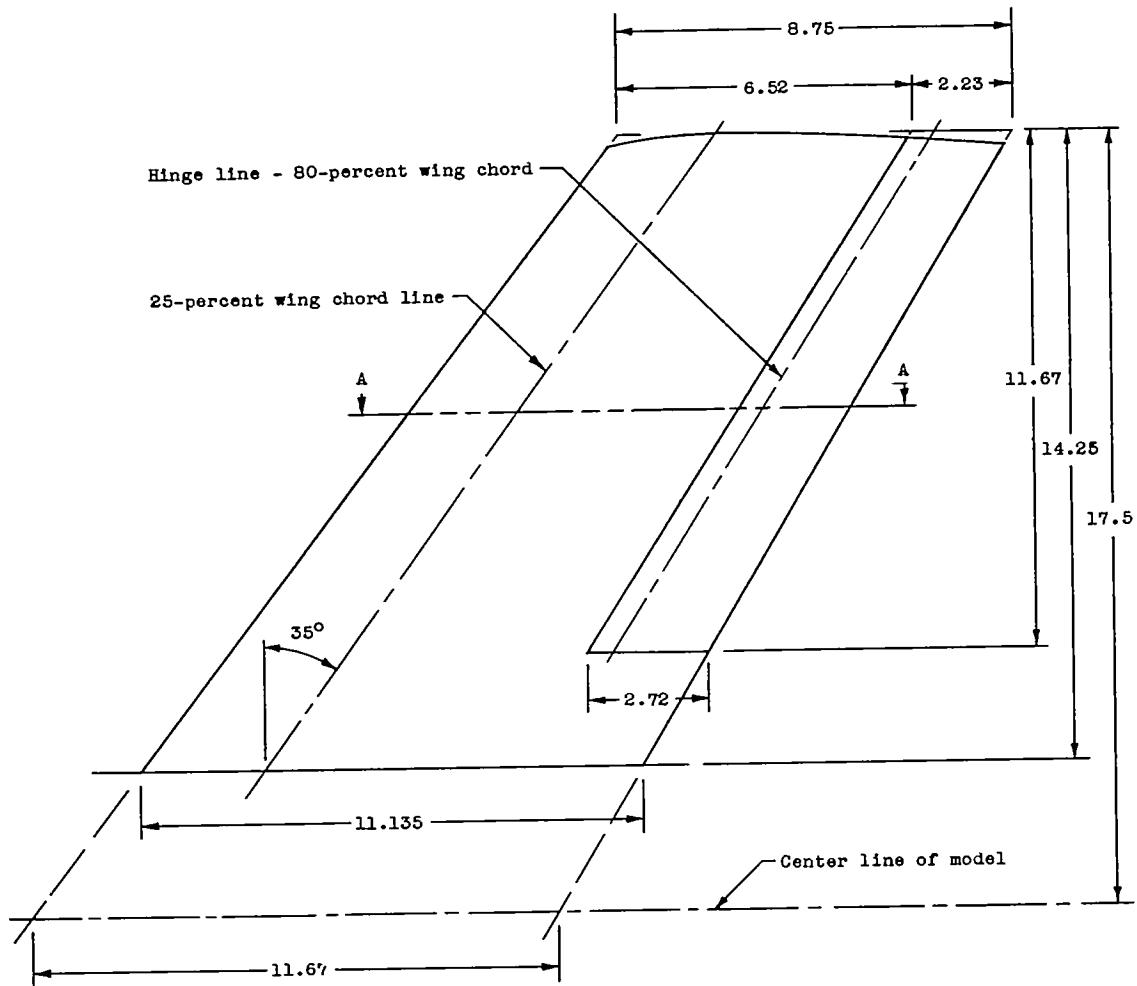
(b) Plan form of swept wing with control surface.

Figure 2.- Concluded.
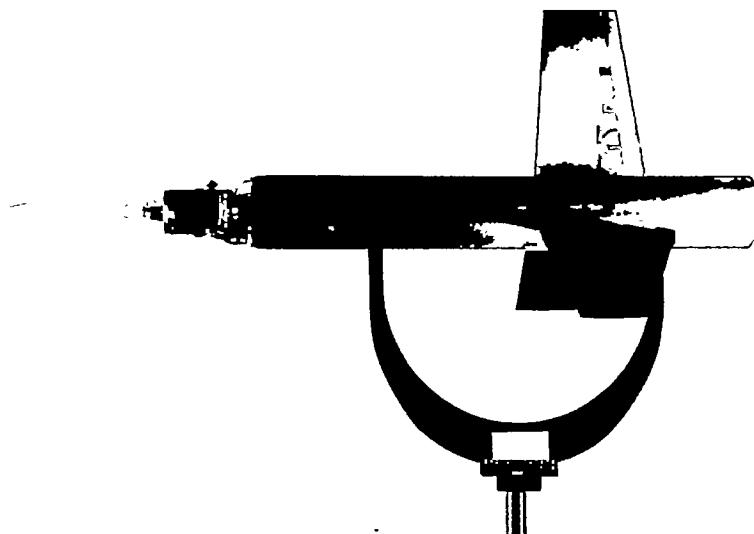
L-76098

(a) Complete model.
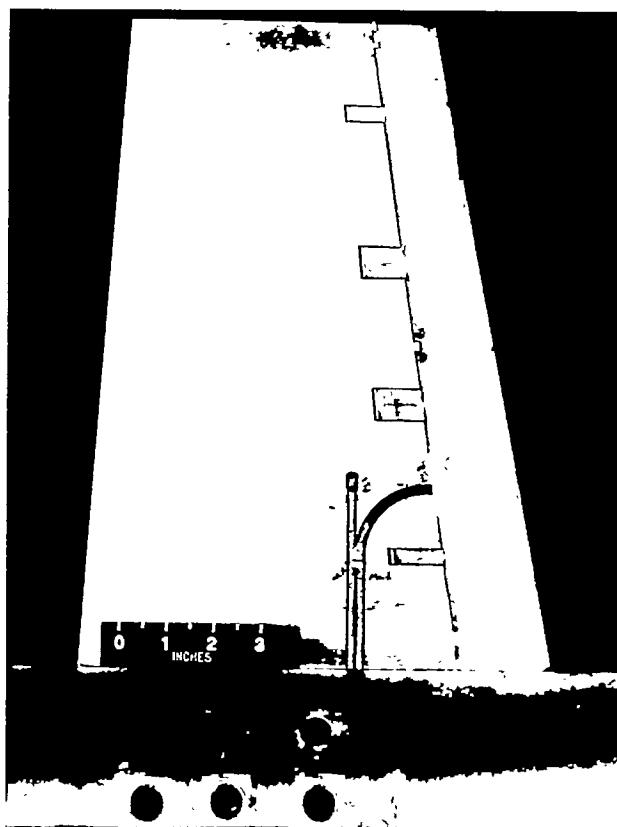
L-76099

(b) Unswept wing showing detail of control surface and pressure orifices.

Figure 3.- Photographs of unswept-wing model.
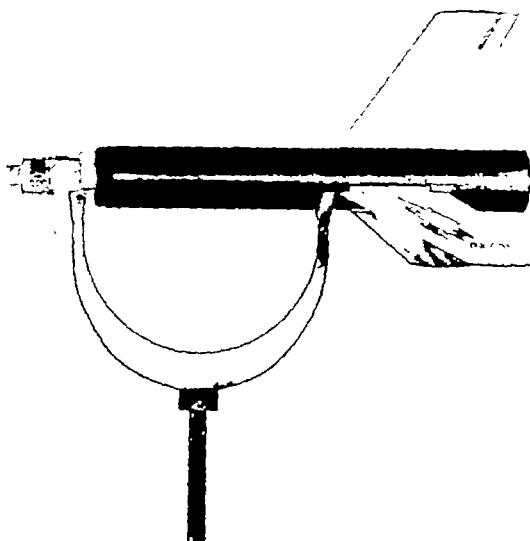
L-71217

(a) Complete model.
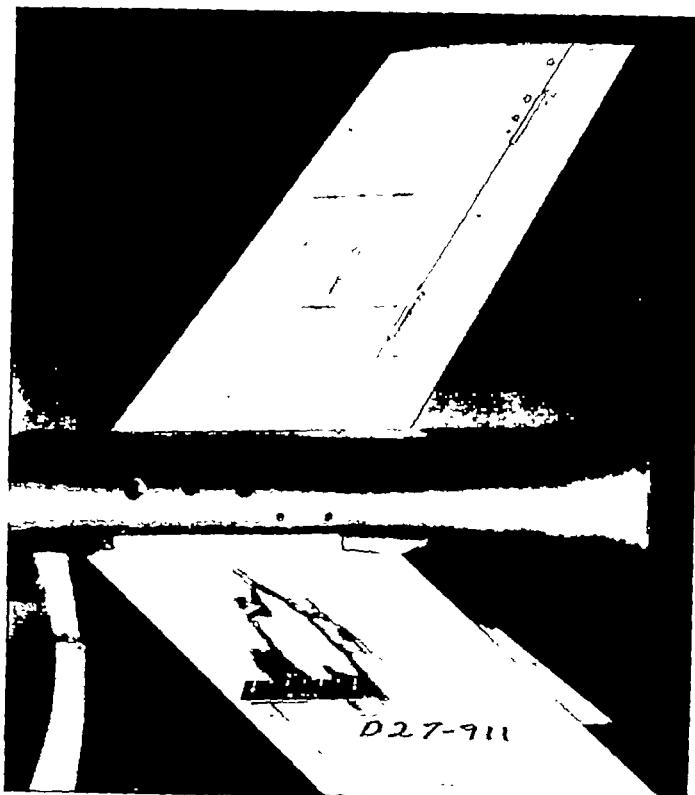
L-71218

(b) Swept wing showing detail of control surface.

Figure 4.- Photographs of typical swept-wing model.
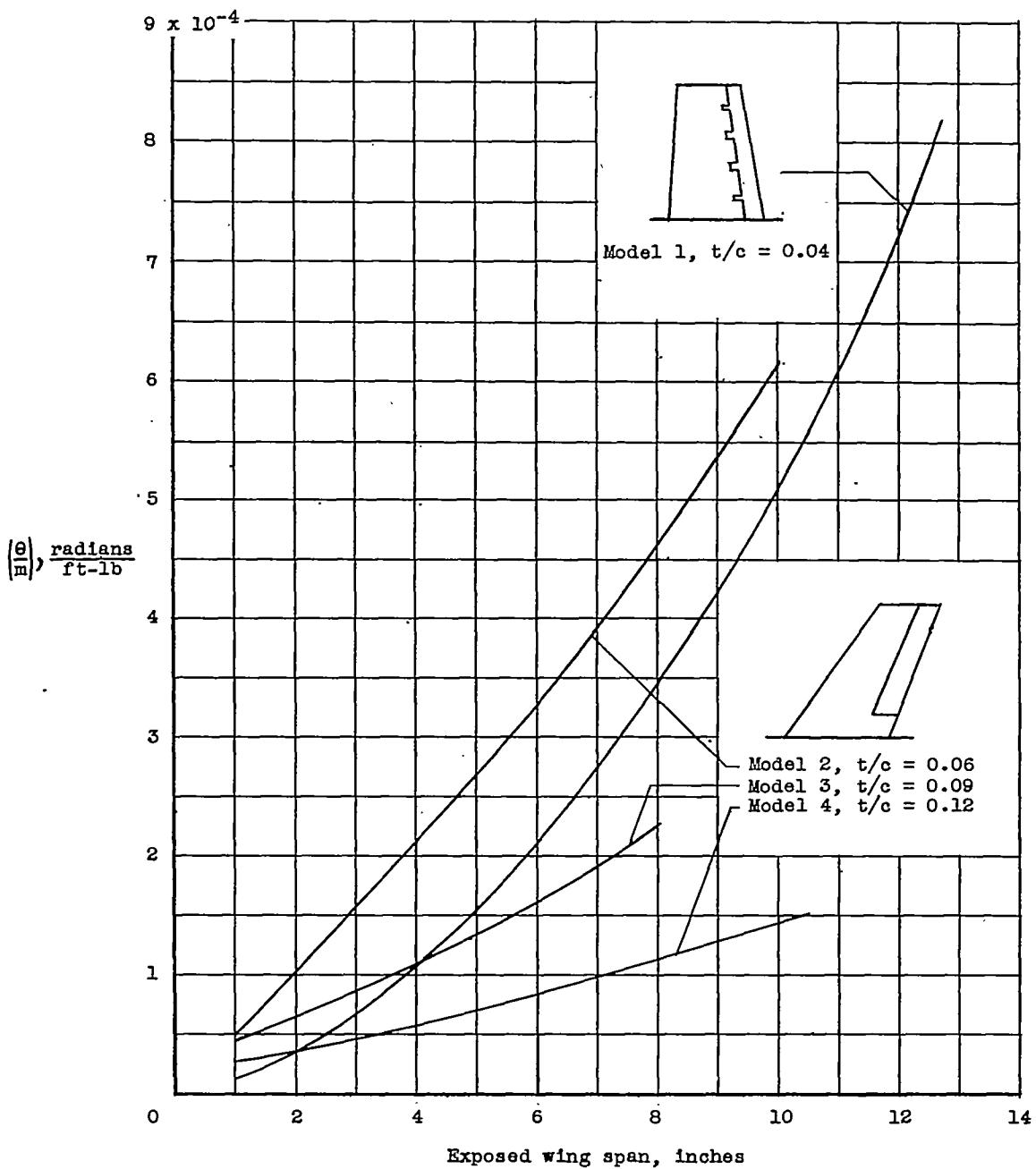
Figure 5.- Variation of wing stiffness parameter with wing span for each model.
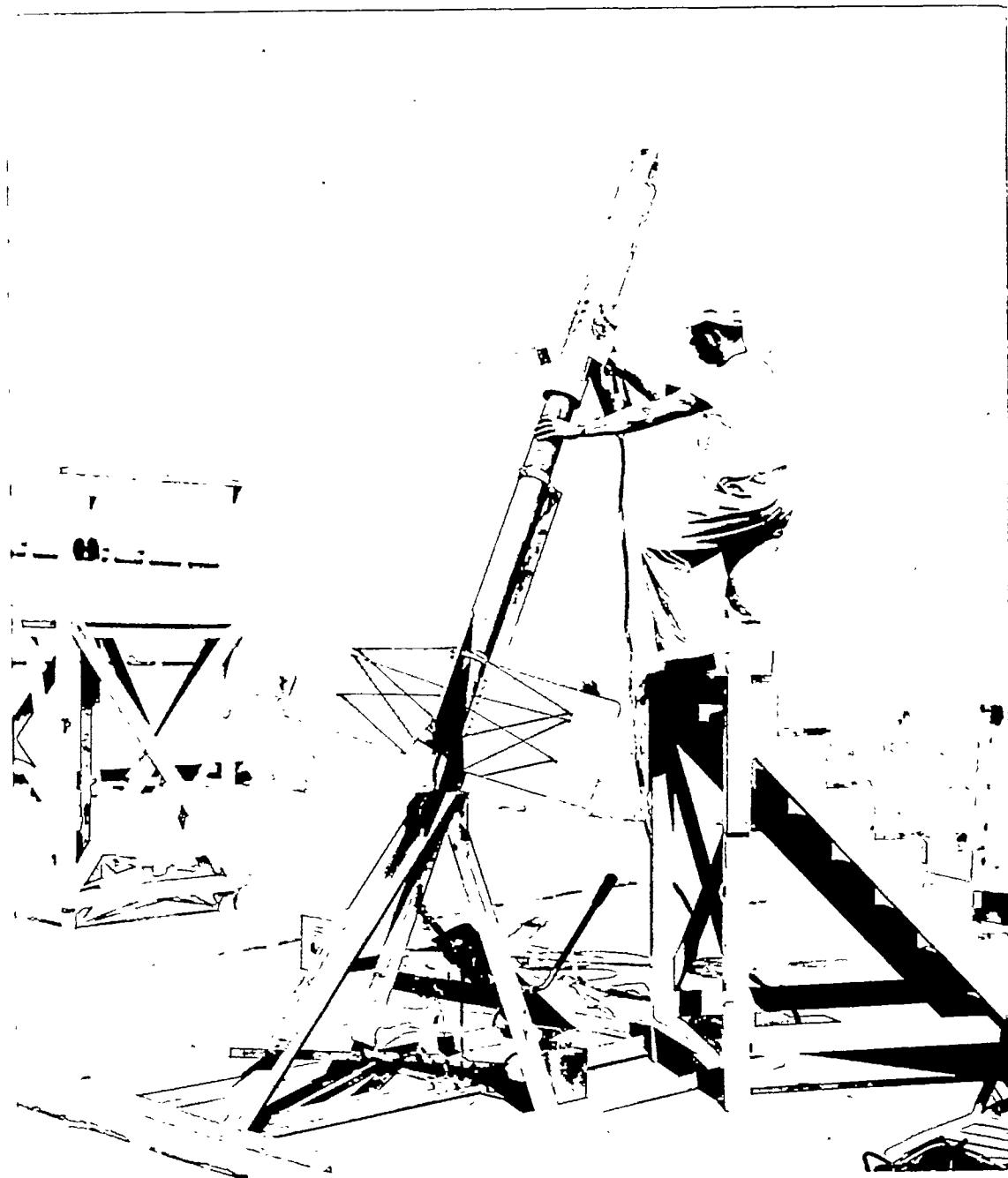
L-71568

Figure 6.- Photograph of a typical model on launcher.
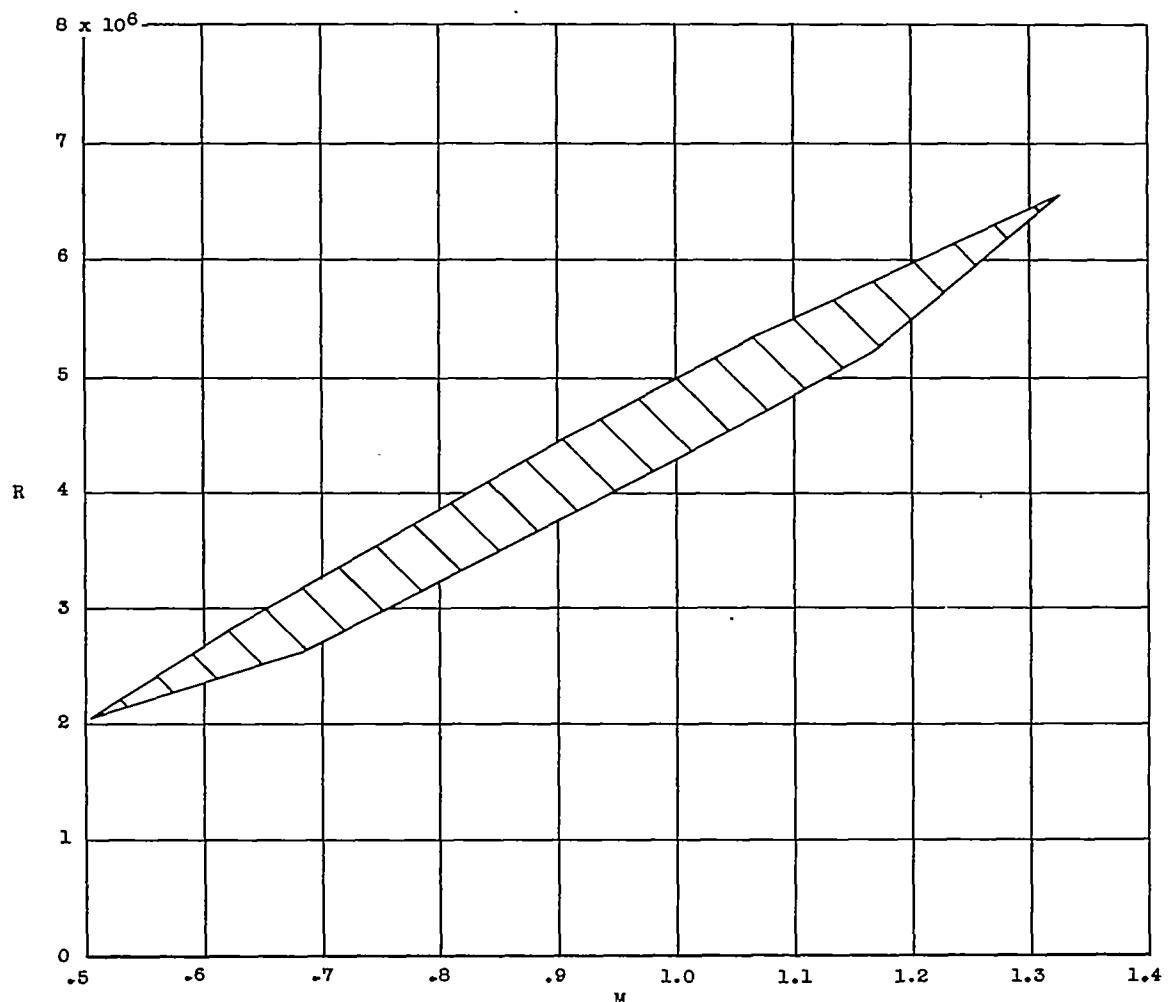
Figure 7.- Variation of Reynolds number with Mach number as based on the
mean aerodynamic chord.

CONFIDENTIAL
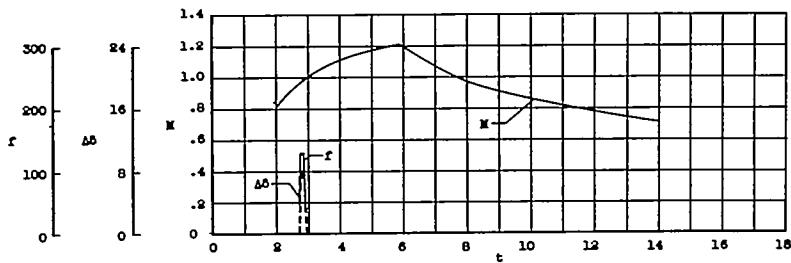
(a) Model 1; $\frac{t}{c} = 0.04$; $\Lambda = 0^{\circ}$.
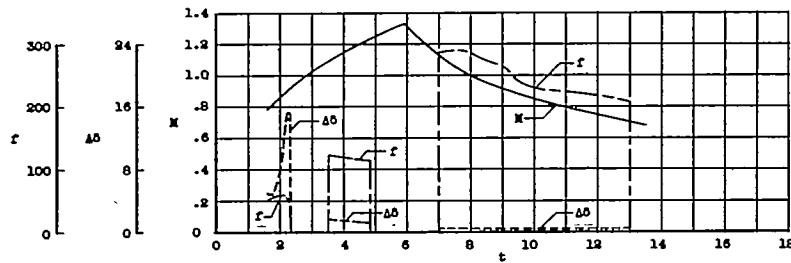
(b) Model 2; $\frac{t}{c} = 0.06$; $\Lambda = 35^{\circ}$.
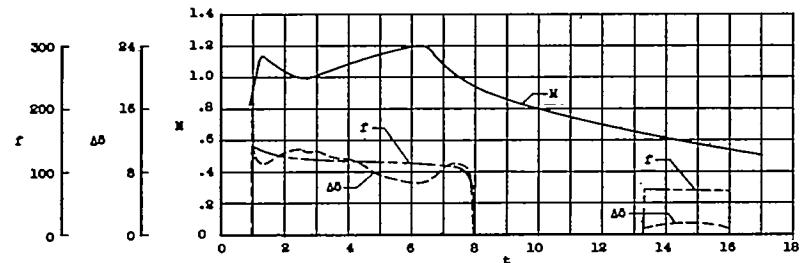
(c) Model 3; $\frac{t}{c} = 0.09$; $\Lambda = 35^{\circ}$.
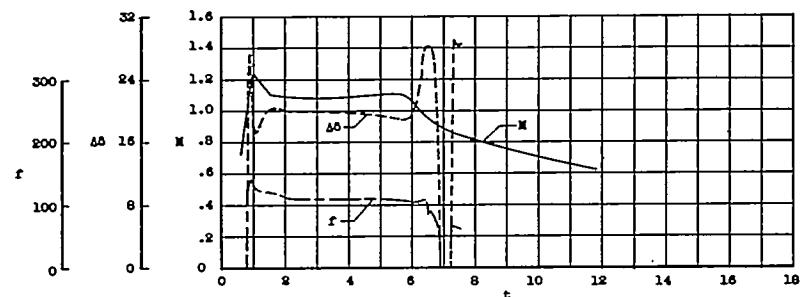
(d) Model 4; $\frac{t}{c} = 0.12$; $\Lambda = 35^{\circ}$.

Figure 8.- Variation of Mach number, total control-surface amplitude, and control-surface frequency with time for each model.

CONFIDENTIAL

t = 2.53 2.74 2.92 3.20
M = .930 .968 .997 1.037

Longitudinal Accelerometer

δ = 1.25° .25° .80° .78°

Control-Surface Position Δδ = 8.0°

130 cps

Static Pressure No. 2 2.62 lb/in²
4.05 lb/in²

Static Pressure No. 1 1.45 lb/in²
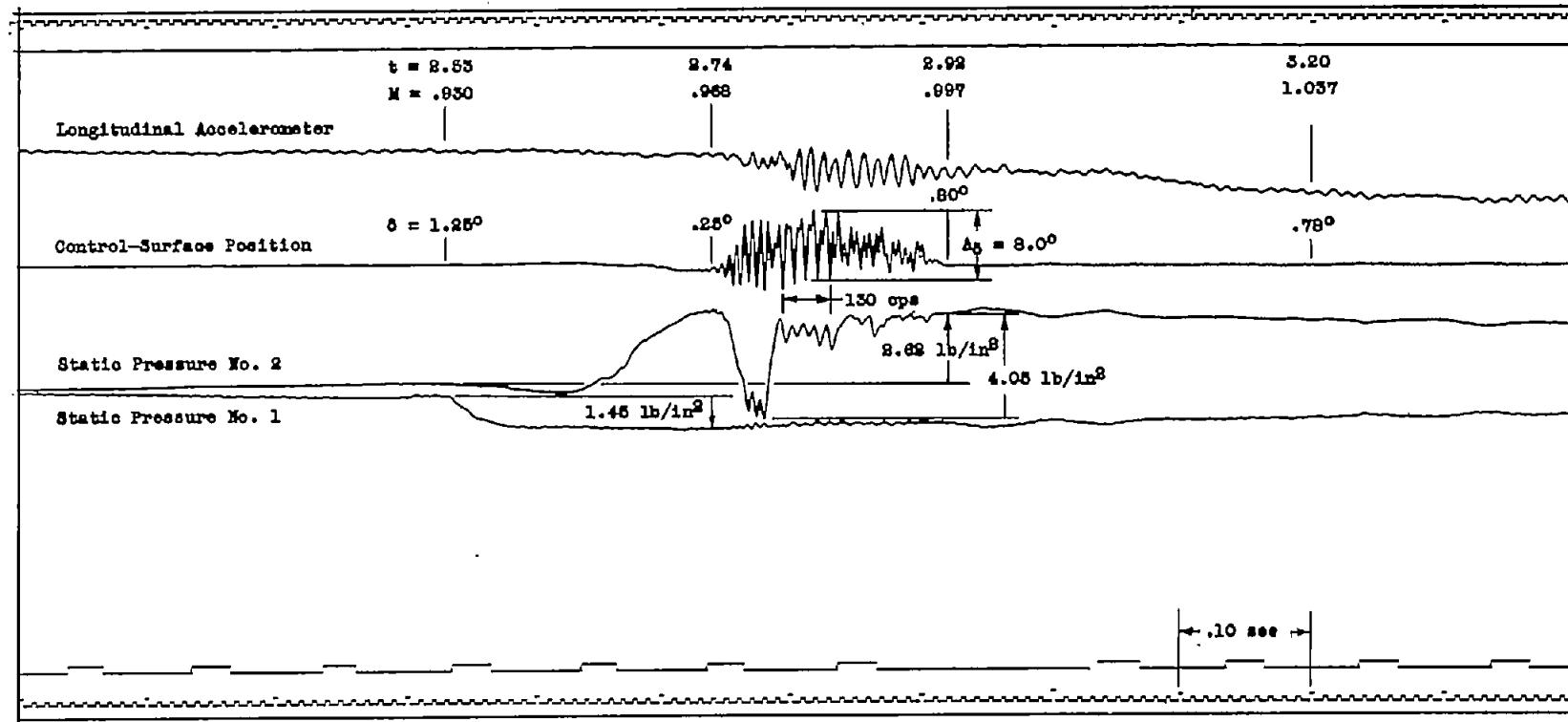
.10 sec

Figure 9.- Section of telemeter record from model 1 $\left(\Lambda = 0°; \frac{t}{c} = 0.04\right)$ showing buzz and pressure differences.

t = .96   .98

M = .883   .903

δ = -1.80° -.63°

t = 1.19

1.137

-.45°

t = 1.40

1.120

-.34°

Control-Surface Position

δ_δ = 16.0°

9.25°

9.08°

Longitudinal Accelerometer

Booster burnout

|←130 cps→|

|←140 cps→|

|←132 cps→|

|←.10 sec.→|
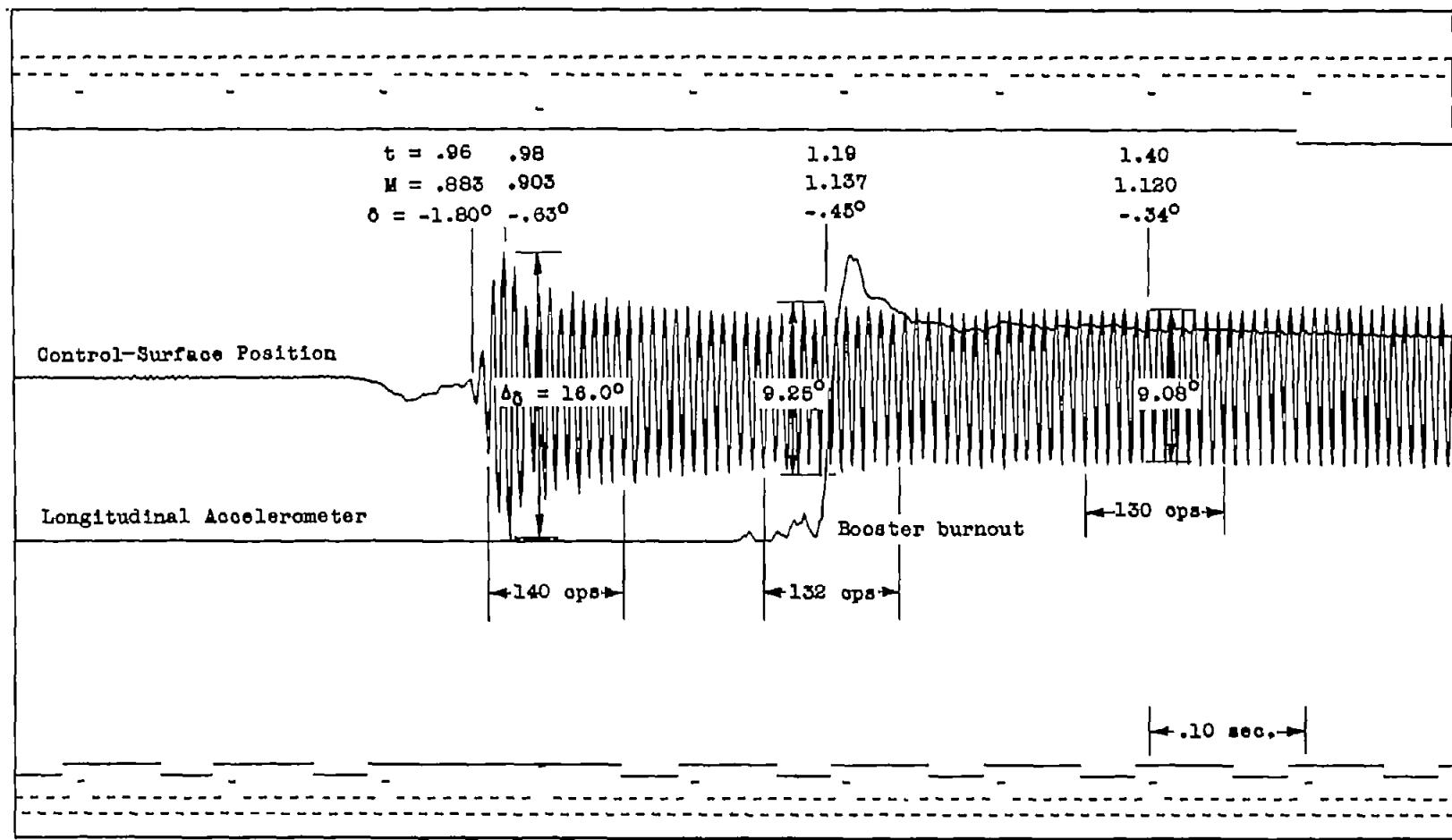
(a) Start of buzz.

Figure 10.- Sections of telemeter record from model 3. $\Lambda = 35°$; $\frac{t}{c} = 0.09$.

t = 2.40   2.65   2.90

$M = 1.001$ .990   1.002

$\delta = -.31°$ $-.30°$ $-.20°$

Control-Surface Position

$\Delta_\delta = 10.86°$ 10.5°   10.7°

|←132 cps→| Sustainer fired   Longitudinal Accelerometer

|←120 cps→| |←119 cps→|

|←.10 sec.→|
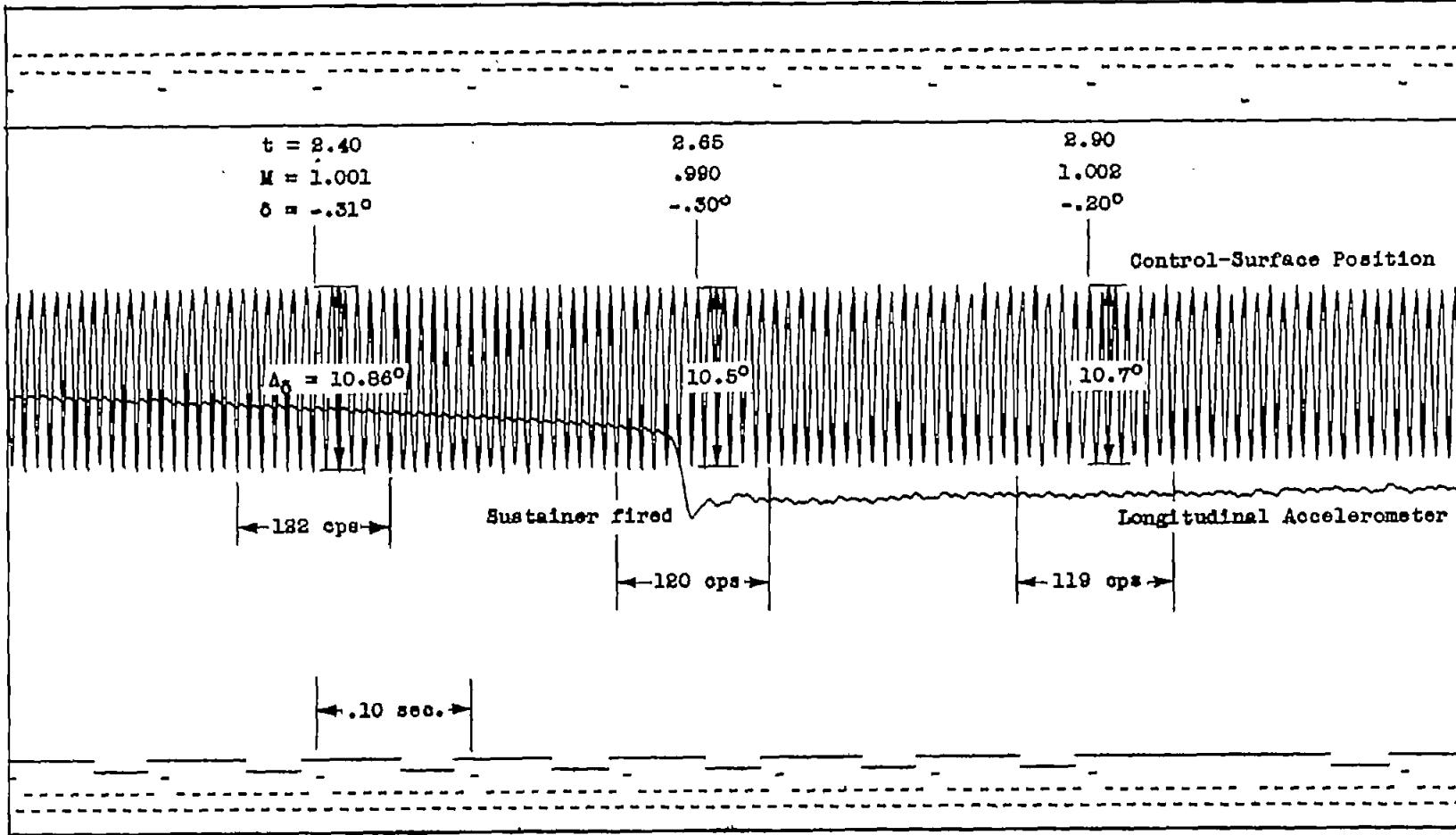
(b) Effect on buzz of change from deceleration to acceleration.

Figure 10.- Continued.
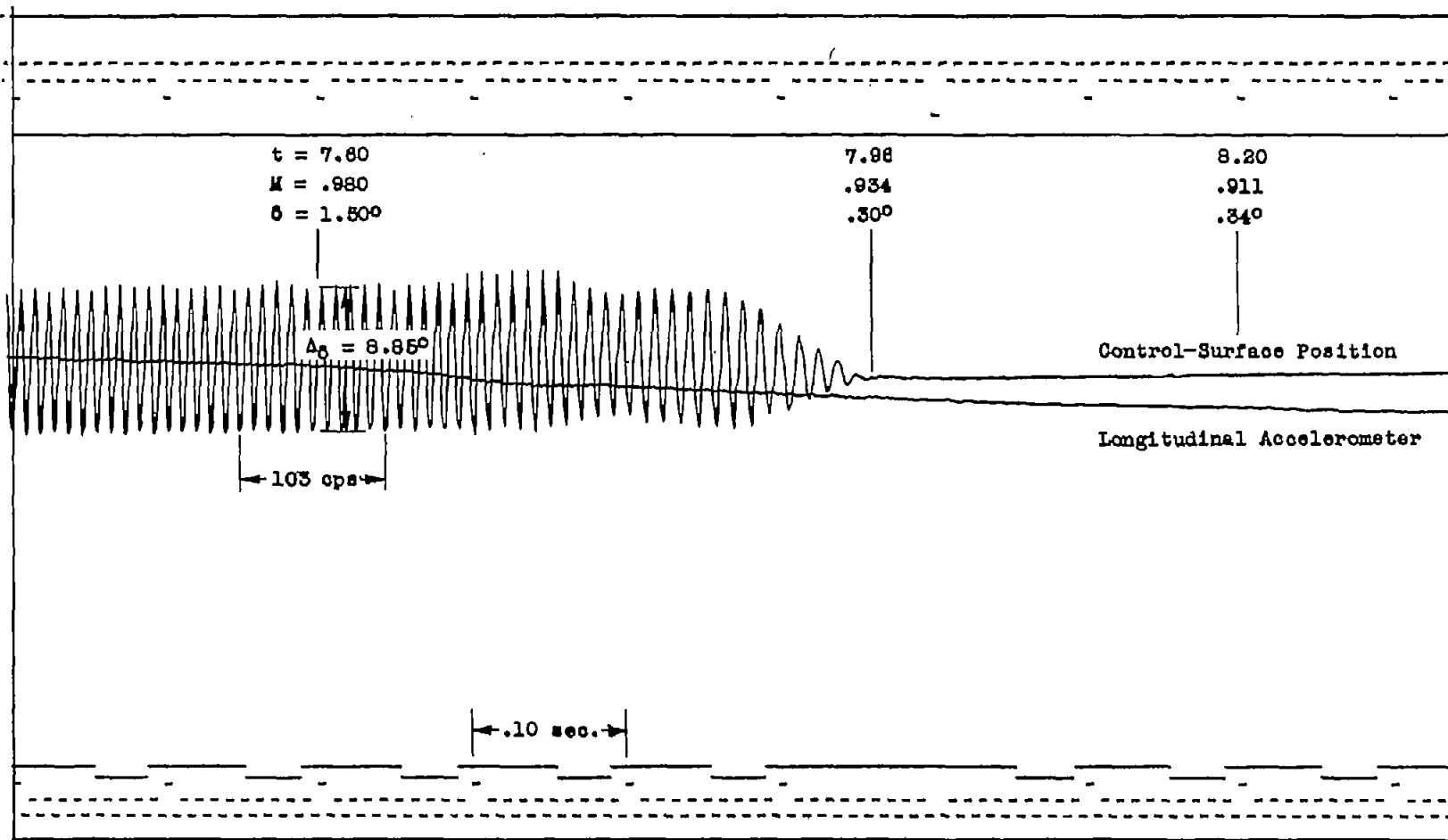
(c) End of buzz.

Figure 10.- Concluded.

t = 6.52	6.72	6.88	7.23	7.48
M = .945	.916	.897	.868	.849
δ = -1.33	-1.15	1.90	-.25	-1.50

Longitudinal Accelerometer

Control-Surface Position

Aδ = 25.80°

29.4°

72 cps

72 cps

.10 sec.

63 cps

63 cps
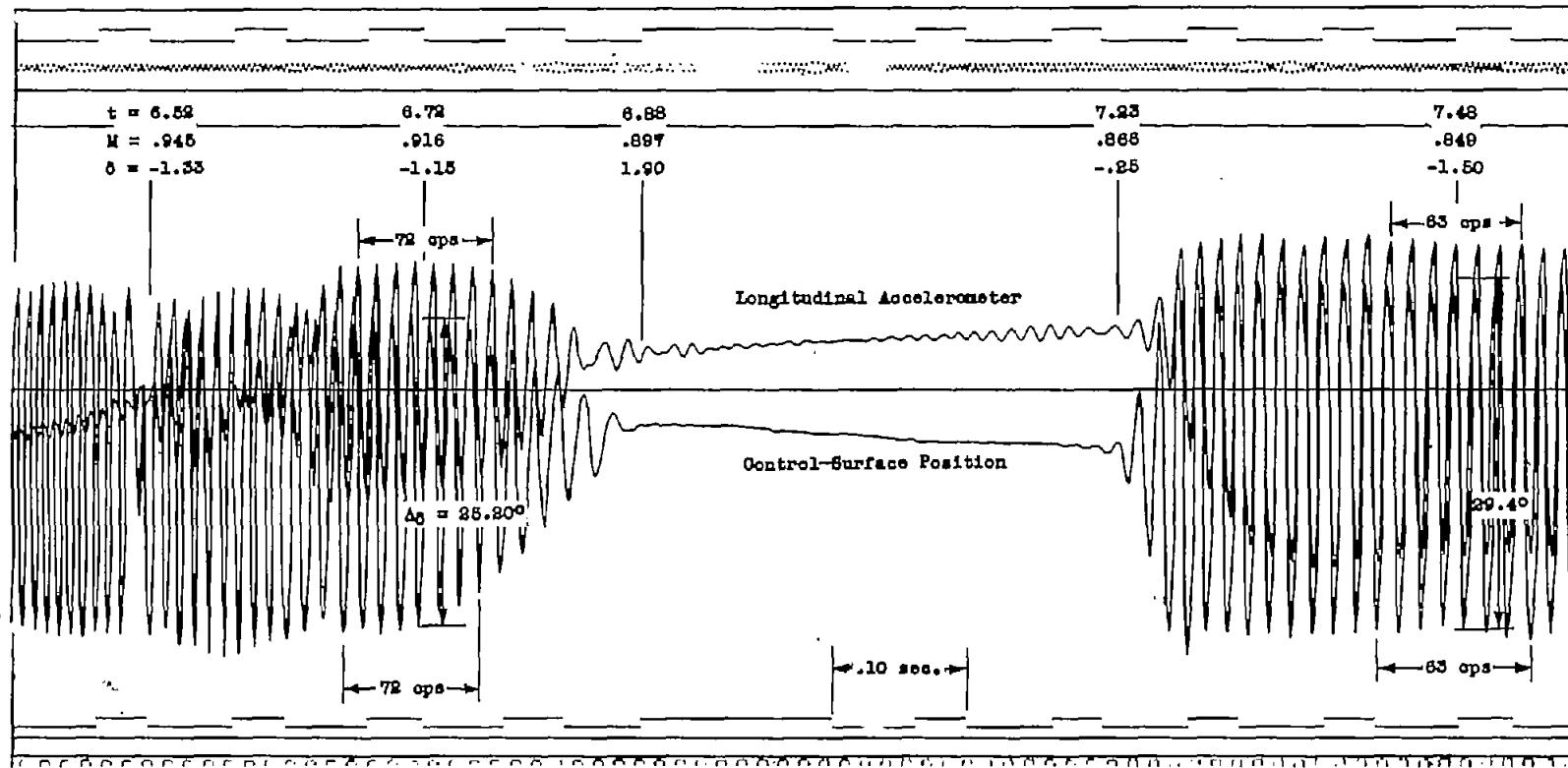
Figure 11.- Section of telemeter record from model 4 $\left(\Lambda = 35°; \frac{t}{c} = 0.12\right)$ showing control-surface and accelerometer vibration.
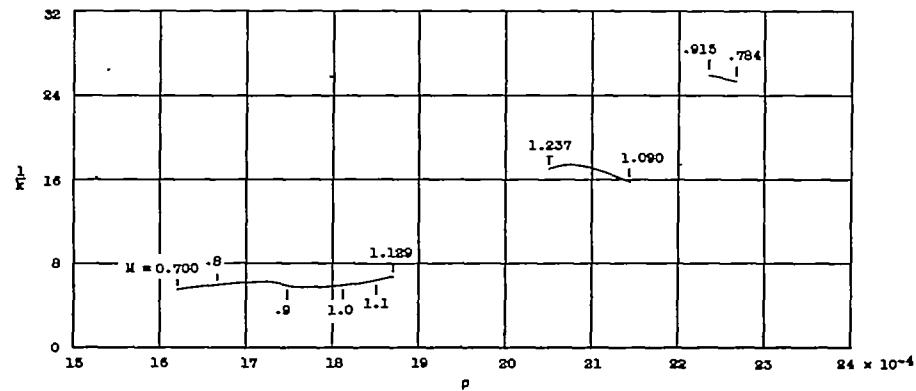
(a) Model 2, $\dfrac{t}{c} = 0.06$.
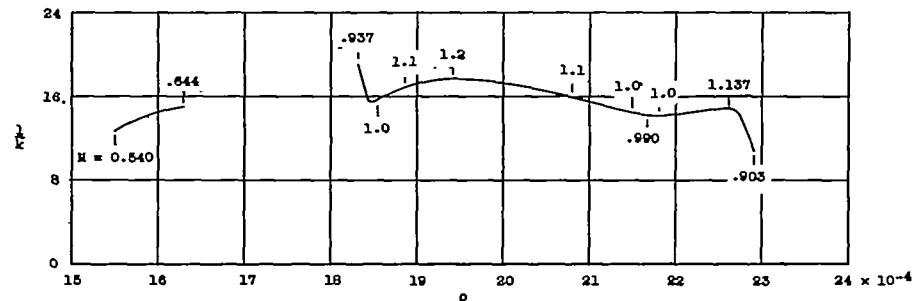
(b) Model 3, $\dfrac{t}{c} = 0.09$.
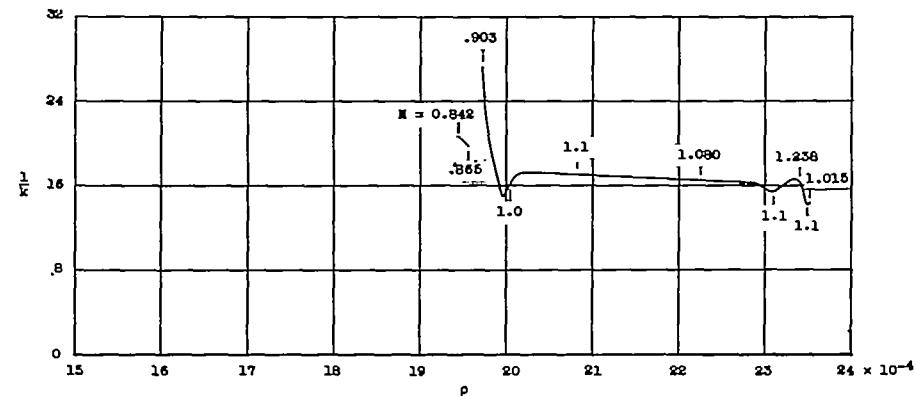
(c) Model 4, $\dfrac{t}{c} = 0.12$.

Figure 12.- Variation of reduced velocity parameter with density for the 6-, 9-, and 12-percent-thick swept wing models.
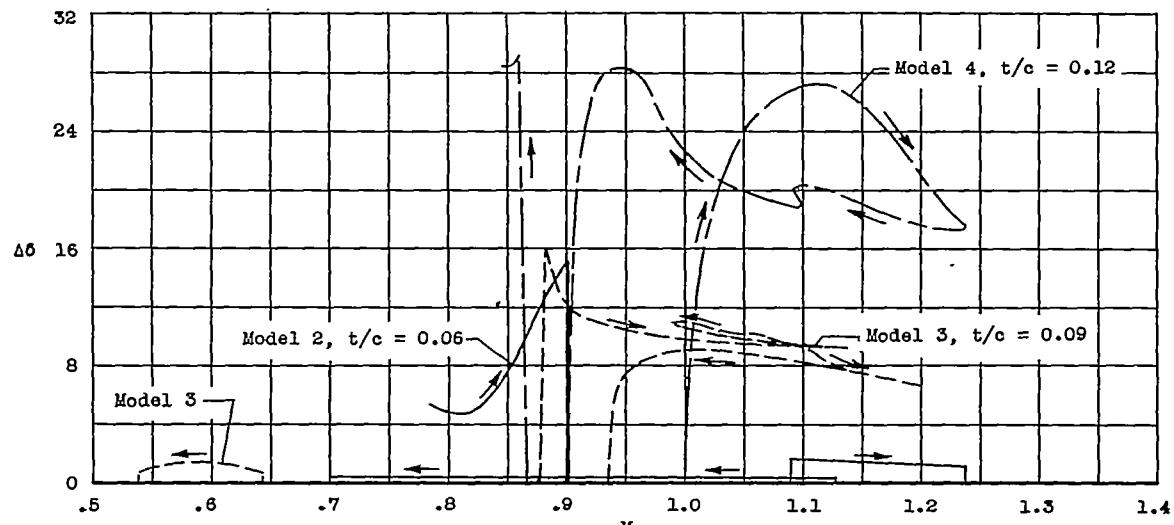
(a) Mach number.
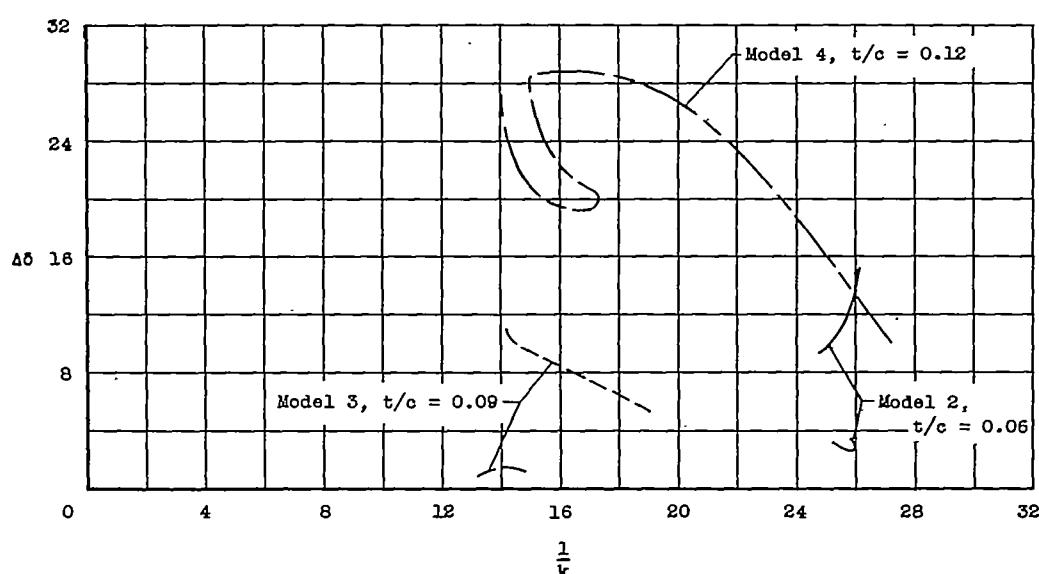
(b) Reduced velocity.

Figure 13.- Variation of control-surface amplitude with Mach number and
reduced-velocity parameter for the 6-, 9-, and 12-percent-thick swept
wings.
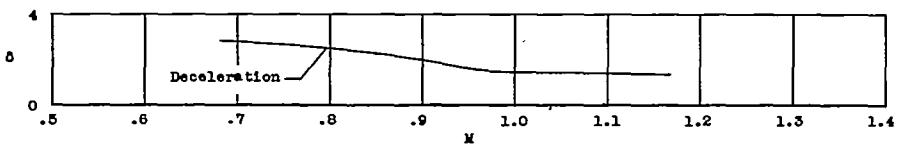
(a) Model 1; $\frac{t}{c} = 0.04$; $\Lambda = 0°$.

(b) Model 2; $\frac{t}{c} = 0.06$; $\Lambda = 35°$.

(c) Model 3; $\frac{t}{c} = 0.09$; $\Lambda = 35°$.

(d) Model 4; $\frac{t}{c} = 0.12$; $\Lambda = 35°$.

Figure 14.- Variation of control-surface trim angle with Mach number for each model.

Figure 15.- Variation of pressure coefficient with Mach number for model 1. $\frac{t}{c} = 0.04$; $\Lambda = 0^{\circ}$.
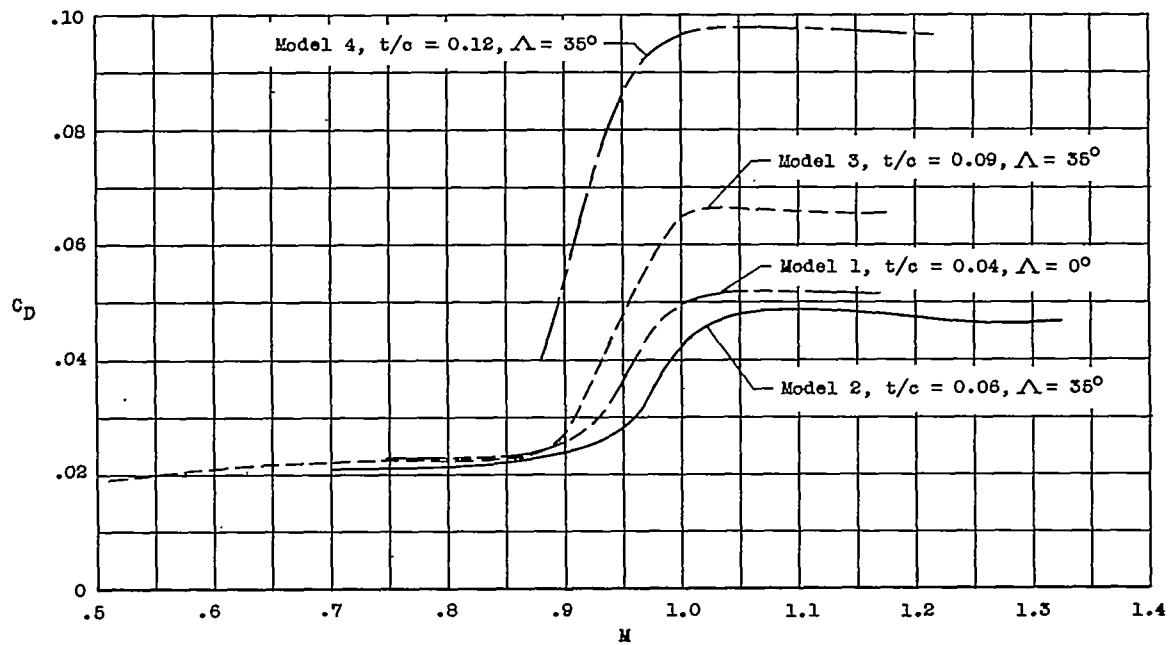

Figure 16.- Variation of drag coefficient with Mach number for each model as based on the total exposed wing area.